Relationship between Chemical Bonding Nature and Electrochemical Property of $LiMn_2O_4$ Spinel Oxides with Various Particle Sizes: "Electrochemical Grafting" Concept

Nadine Treuil,[†] Christine Labrugère,[†] Michel Menetrier,[†] Josik Portier,[†] Guy Campet,*[,†,||] Anne Deshayes,[‡] Jean-Claude Frison,[§] Seong-Ju Hwang,[#] Seung-Wan Song,[#] and Jin-Ho Choy*[,#,⊥]

Institut de Chimie de la Matière Condensée de Bordeaux (ICMCB) du CNRS, Château Brivazac, avenue du Dr. A. Schweitzer, 33608 Pessac, France, Centre National d'Etudes des Télécommunications (CNET), 38-40 rue du Général Leclerc, 92131 Issy-les Moulineaux, France, CNET, 2 route de Trégastel, BP40, 22301 Lanion, France, and Department of Chemistry, Center for Molecular Catalysis, College of Natural Sciences, Seoul National University, Seoul 151-742, Korea

Received: November 5, 1998; In Final Form: January 9, 1999

Systematic Mn 2p XPS and Mn K-edge XAS analyses together with the electrochemical measurement have been carried out for the spinel $LiMn_2O_4$ prepared at various sintering temperatures in order to elucidate an origin of the dependence of electrochemical properties on synthetic conditions. From the comparative experiments, it becomes clear that a lowering of synthetic temperature gives rise to an increase of structural disorder and of the average oxidation state of manganese, which is more prominent on the surface than in the bulk. Such results suggest that the modification of surface property induced by a decrease of particle size is closely related to the electrochemical performance. The nanocrystalline $LiMn_2O_4$ prepared at 250 °C shows excellent cyclability at the 3 V region compared to that of microcrystalline $LiMn_2O_4$ prepared at 700 °C. For the purpose of examining the evolution of the chemical bonding nature of inserted lithium, ^{7}Li MAS NMR studies have been performed for both the spinel compounds before and after Li^+ intercalation. While the intercalation of 0.2 mol Li^+ does not induce any remarkable spectral change for the microcrystalline $LiMn_2O_4$, it leads to a dramatic suppression of the NMR signal for the nanocrystalline $LiMn_2O_4$, indicating that the process of grafting Li into the latter phase results in significant modifications of the chemical environment of lithium. On the basis of present experimental findings, it can be concluded that the lowering of synthetic temperature modifies the surface properties, which facilitates the grafting process of Li^+ ion and, thereby, enhances the electrochemical properties for the 3 V region corresponding to the Li insertion.

Introduction

The low cost and environmental benignancy of manganese have created intense research interest in the $LiMn_2O_4$ spinel as a promising cathode material for rechargeable lithium batteries.[1−4] However, the $LiMn_2O_4$ spinel has some disadvantages such as inferior theoretical capacity (148 mAh/g compared to 274 mAh/g for $LiNiO_2$) and unacceptable performance fade, which frustrate a commercial use of this cathode material. To overcome these shortcomings, the electrochemical properties of the $LiMn_2O_4$ spinel have been extensively investigated by controlling various factors such as synthetic procedure and conditions, substitution of aliovalent cations, etc.[1−10] Recently we have established that the nanocrystalline $LiMn_2O_4$ sample with an average crystallite size lower than 10 nm exhibits an excellent cyclability for the 3 V cell, whereas it shows a severe capacity loss for the 4 V one, respectively.[9,10] This is very consistent with the previous "electrochemical model" where nanocrystalline materials are predicted to have an enhanced electrochemical activity, compared to that of their microcrystalline homologues, in case the first electrochemical process is a discharge of the Li battery.[11,12] However, such a theoretical model has not been confirmed yet for the $LiMn_2O_4$ cathode material. In this respect, the evolution of crystal structure and electronic configuration of this compound upon lowering of synthetic temperature and Li insertion should be carefully investigated to obtain direct evidence of the mechanism of Li insertion. In the case of nanocrystalline materials, X-ray absorption spectroscopy (XAS) is expected to be the most effective tool for probing the chemical environment of metal atom, since it does not require a long-range structural order.[13−15] Moreover, a combination of XAS and X-ray photoelectron spectroscopy (XPS) enables us to differentiate the electronic structure of chemical species in bulk and on the surface, which would be useful in studying the effects of grafting and intercalation processes.[15−19]

In this work, combinative XPS and XAS analyses together with electrochemical measurements have been carried out for the $LiMn_2O_4$ spinel oxides prepared at various temperatures to examine the effect of particle size on the electronic and local geometrical structures and electrochemical properties. The evolution of the chemical environment of lithium upon intercalation has also been investigated by performing the ^{7}Li NMR experiments for the pristine $LiMn_2O_4$ spinel oxides and their Li intercalates, because they allow us to probe the very site

* Authors to whom correspondence should be addressed.
[†] ICMCB-CNRS.
[‡] CNET, Issy-les Moulineaux.
[§] CNET, Lanion.
[#] Seoul National University.
[||] Tel: +33-5-56-84-62-79. Fax: +33-5-56-84-27-61. E-mail: campet@icmcb.chimsol.u-bordeaux.fr.
[⊥] Tel: +82-2-880-6658. Fax: +82-2-872-9864. E-mail: jhchoy@plaza.snu.ac.kr.

10.1021/jp984316t CCC: $18.00
Published on Web 03/06/1999

occupied by lithium as well as the oxidation state of the neighboring metal ion.[20−26]

Experimental Section

Sample Preparation and Characterization. The polycrystalline samples of $LiMn_2O_4$ with different particle sizes have been prepared by the coprecipitation method where the aqueous solution of $Mn(CH_3COO)_2 \cdot 4H_2O$ and Li_2CO_3 was agitated for 1 h and dehydrated at 85 °C, and the resulting powder was heated at various temperatures in an ambient atmosphere. The formation of single phase $LiMn_2O_4$ spinel oxides was confirmed by X-ray diffraction (XRD) measurements using Ni-filtered CuKα radiation with a graphite diffracted beam monochromator.

Electrochemistry. The electrochemical measurements were performed using a computer-controlled potentiostat/galvanostat (Tacussel, PGS 201T model) for the electrochemical cells based on the "Li/liquid electrolyte/composite electrode". The Li anode is a lithium metal foil (Aldrich 99.9%). The liquid electrolyte consists of 1 M $LiPF_6$ (Aldrich 99.99%) dissolved in a solution of ethylene carbonate (EC, Prolabo 99%) + dimethyl carbonate (DMC, Aldrich 99%) (50/50 by volume). The composite cathodes were prepared by mixing the lithium manganese oxide together with Chevron carbon black and a binder, poly(tetrafluoroethylene) (i.e., Teflon), in the weight ratios 80:13:7. The mixture was then pressed at 1 ton/cm^2 for 1 min and the resulting pellet was finally dried under primary vacuum for 15 h at 120 °C. All manipulations of air-sensitive materials as well as the cell assemblies were carried out in the inert atmosphere of an argon-filled glovebox.

X-ray Photoelectron Spectroscopy. The present XPS data were collected using a VG 220i-XL Escalab spectrometer with a monochromatized AlKα source ($h\nu = 1486.6$ eV) and a spot size of about 500 μm. The pressure in the analysis chamber during measurements was maintained in the 10^{-8} Pa range. The powdered samples were pressed onto small indium foils, from which the Mn 2p signals were obtained in the constant pass energy mode of 20 eV. To determine quantitatively an oxidation state of manganese, the experimental spectra were fitted by using a Shirley background function and a nonlinear least-squares fitting software provided by VG Scientific. The binding energies were calibrated by fixing the C 1s line of residual carbon at 285 eV on a silver crystal (Ag $3d_{5/2} = 368.28$ eV) with an accuracy of ±0.1 eV.[27]

X-ray Absorption Spectroscopy. The XAS experiments were performed with synchrotron radiation by using extended X-ray absorption fine structure (EXAFS) facilities, installed at the beam line 3C1 at the Pohang Light Source (PLS) in Pohang, operated at 2 GeV with a ring current of ~100 mA. The samples were finely ground, mixed with boron nitride (BN) in an appropriate ratio, and pressed into pellets in order to obtain an optimum absorption jump ($\Delta\mu t \cong 1$) enough to be free from the thickness and pinhole effects.[28,29] All the present spectra were obtained at room temperature in a transmission mode using gas-ionization detectors with a spacing of ~0.4 eV for the X-ray absorption near-edge structure (XANES) region and ~1.5 eV for the EXAFS one. The synchrotron X-ray beam was monochromatized with a channel-cut silicon (111) crystal. All the present spectra were calibrated by measuring the spectrum of a Mn metal foil and by fixing the first absorption peak to 6539 eV.

The data analysis for the experimental spectra was performed by standard procedures as reported previously.[13] All the present XANES spectra were normalized by fitting the smooth EXAFS high-energy region with a linear function after subtracting the background extrapolated from the preedge region. The EXAFS oscillations were separated from the absorption background by using a cubic spline background removal technique. The resulting $\chi(k)$ oscillations were weighted with k^3 in order to compensate for the diminishing amplitude of the EXAFS at high k region. For analyzing the EXAFS data, a nonlinear least-squares curve fitting was carried out to the Fourier filtered coordination shells by minimizing the value of F ($F = [\sum k^6 (\chi_{cal} - \chi_{exp})^2]^{1/2}/n$, where the summation was performed over the data points (n) in the analyzed k range) with the use of well-known single scattering EXAFS theory.[30]

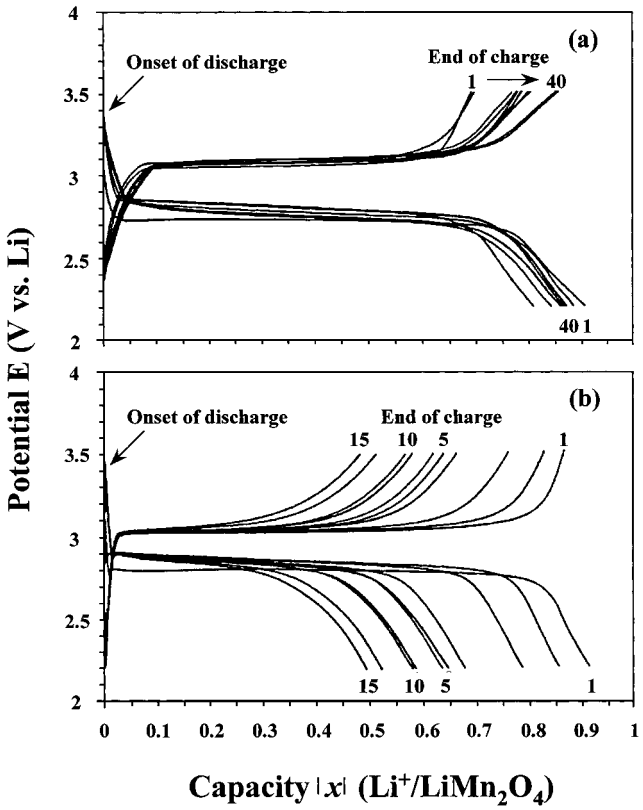

Figure 1. Galvanostatic discharge−charge curves for (a) **LT** and (b) **HT**, at 500 μA in "Li/EC-DMC, 1 M $LiPF_6$/3 V $LiMn_2O_4$" cells, at 25 °C (cathode active mass = 20 mg; effective area = 1.33 cm^2).

^{7}Li MAS NMR Measurement. The present ^{7}Li NMR spectra were recorded at 77.7 MHz and 4.7 T using a Bruker MSL 200 spectrometer. Magic angle spinning (MAS) was used with the spinning speed frequency range of 10−15 kHz in a commercial Bruker probehead. Due to the residual width of the signal in some cases, a solid echo sequence was applied with a synchronization of the interpulse delay to the rotor period. The duration of the two pulses was fixed at 2.5 μs, leading to a flip angle close to 90°. The repetition time was maintained at 1 s. A 1 M solution of LiCl was used as an external reference. To determine the isotopic positions of the MAS pattern, the spinning speed was varied.

Results and Discussion

Electrochemistry. Figures 1 and 2 represent the capacity−potential profiles of the $LiMn_2O_4$ compounds prepared at 250 °C (denoted as **LT**) and 700 °C (denoted as **HT**) for the potential ranges of 2.5−3.5 V and 3.5−4.5 V (vs Li/Li$^+$), respectively. As shown in Figure 1, the **LT** sample exhibits a better electrochemical performance for the 3 V region corresponding to the insertion of lithium than the **HT** sample. That is, as the cycling proceeds, the capacity of the former is first enhanced

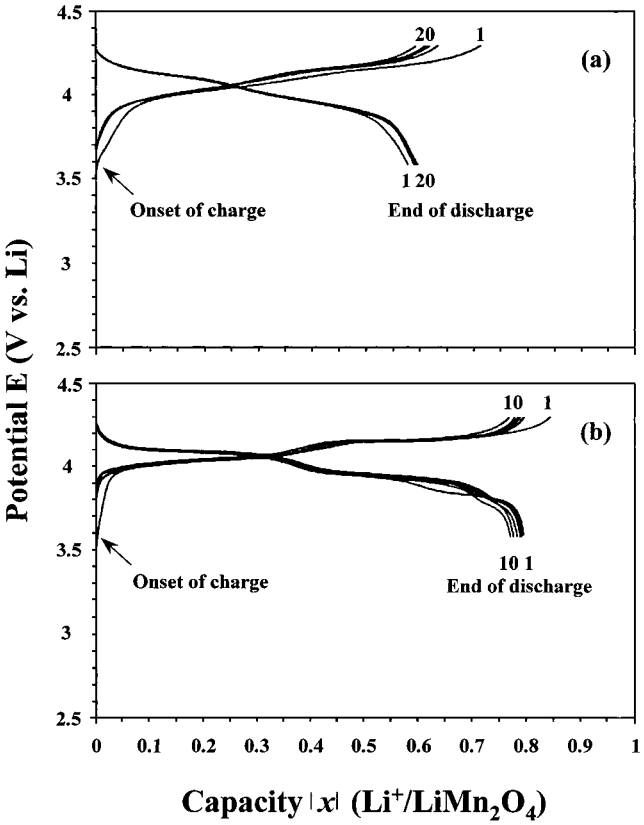

Figure 2. Galvanostatic charge−discharge curves for (a) **LT** and (b) **HT**, at 500 μA in "Li/EC-DMC, 1 M $LiPF_6$/4 V $LiMn_2O_4$" cells, at 25 °C (cathode active mass = 20 mg; effective area = 1.33 cm^2).

then stabilized, whereas that of the latter is remarkably depressed, which is in good agreement with our model.[10,11] On the contrary, the **LT** material shows an inferior lithium deintercalation capacity for the 4 V region corresponding to the extraction of lithium, with respect to the **HT** material (Figure 2). According to our previous observations, such a poor cyclability of **LT** for the 4 V region originates from the fact that the structural defect or distortion, which is richer in this nanosized sample, would inhibit the deintercalation of the Li^+ ions.[10] From the scanning electron microscopy (SEM) measurement,[10] it becomes clear that the lowering of the sintering temperature decreases the crystallite size. Such a change of particle size is thought to modify the crystal structure and electronic configuration of the $LiMn_2O_4$ compound, which is closely related to its electrochemical property.[11] In this respect, the chemical bonding nature of lithium manganates prepared at various temperatures needs to be investigated by performing the combinative XPS and XAS studies, to better clarify the relationship between the crystal size of $LiMn_2O_4$ and its electrochemical property.

Mn 2p XPS Analysis. Figure 3 represents the Mn 2p XPS spectra for $LiMn_2O_4$ compounds with the heat treatment at 250 (**LT**), 500, 600, and 700 °C (**HT**), in comparison with those for the references of $Mn^{+IV}O_2$ (pyrolusite) and $Mn^{+III}{}_2O_3$ (bixbyite). The Mn $2p_{3/2}$ peak of MnO_2 is observed at 642.6 eV, while a rather broad feature is detected for Mn_2O_3 around 642 eV with a large full width at half-maximum of 2.8 eV. Such a peak broadening of the latter suggests that there is a significant Mn^{+IV} concentration in Mn_2O_3, which is attributed to a preferential oxidation of manganese ion stabilized on the surface and/or grain boundary. As shown in Figure 3, all the present $LiMn_2O_4$ compounds exhibit the similar spectral features

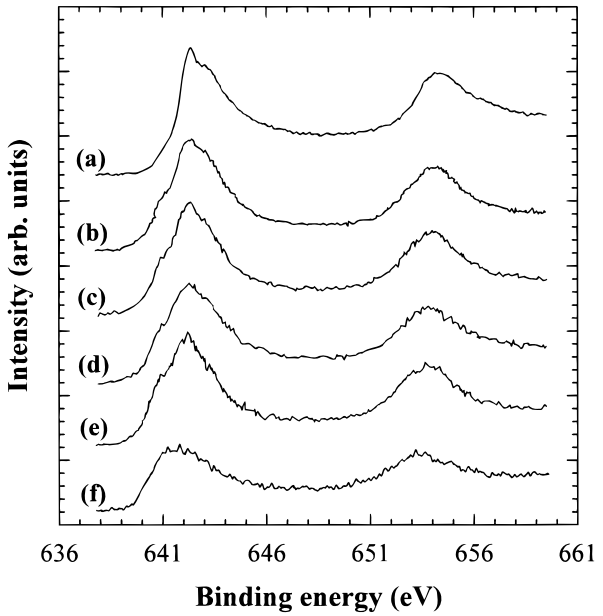

Figure 3. Mn 2p XPS spectra for $LiMn_2O_4$ samples with different sintering temperatures of (b) 250 (**LT**), (c) 500, (d) 600, and (e) 700 °C (**HT**), in comparison with those for the references (a) MnO_2 and (f) Mn_2O_3.

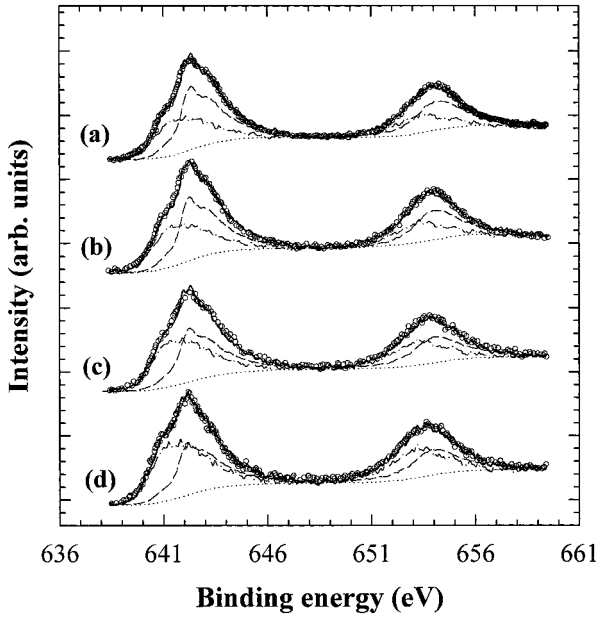

Figure 4. Comparison of the calculated Mn 2p XPS spectra (solid lines) with the experimental data (empty circles) for $LiMn_2O_4$ samples prepared at (a) 250 (**LT**), (b) 500, (c) 600, and (d) 700 °C (**HT**). The dashed, dot−dashed, and dotted lines represent the MnO_2, Mn_2O_3, and background components, respectively.

with a pronounced maximum at 642.7 eV corresponding to Mn^{+IV} species and a distinct shoulder around 641.7 eV corresponding to Mn^{+III} species. To determine the average oxidation state of manganese, the relative ratio of Mn^{+III} and Mn^{+IV} in the lithium manganates has been calculated by least-squares fitting analysis with two spectra of Mn_2O_3 and MnO_2. The best-fitting results are compared with the experimental spectra in Figure 4. And the relative proportions (C_i's) of Mn^{+III} and Mn^{+IV}, defined as the equation of $C_i = S_i/\Sigma_i S_i$ where S_i is the peak area associated to each component, are summarized in Table 1. The present results clarify that the average oxidation state of manganese is increased as the sintering temperature is lowered. From the relative concentration of both Mn^{+III} and

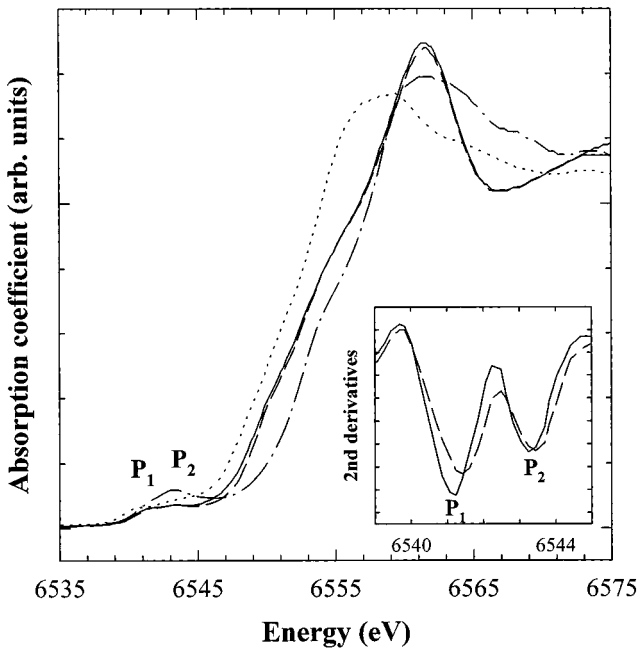

Figure 5. Mn K-edge XANES spectra for **LT** (solid lines) and **HT** (dashed lines), in comparison with those for the references of MnO_2 (dot−dashed lines) and Mn_2O_3 (dotted lines). The inset represents the expanded views of the corresponding second-derivative spectra for the range 6539−6545 eV.

TABLE 1: Relative Proportion of Mn^{+IV} and Mn^{+III} Ions in $LiMn_2O_4$ Samples Prepared at Various Sintering Temperatures

sintering temperature	$S_{Mn^{+IV}}/S_{Mn^{+III}}$	$C_{Mn^{+III}}$	$C_{Mn^{+IV}}$
250 °C	1.4	41.0%	59.0%
500 °C	1.2	44.0%	56.0%
600 °C	1.0	51.1%	48.9%
700 °C	0.8	55.5%	44.5%

Mn^{+IV} ions, the average oxidation state of manganese is determined to be 3.59 for **LT** and 3.44 for **HT**.[31]

Mn K-Edge XANES Analysis. As mentioned above, XPS reflects mainly the chemical species present on the surface, whereas XAS can provide complementary information on the bulk species. In this respect, the XAS analysis has been performed for the lithium manganates with various synthetic temperatures to examine the difference of electronic structure between bulk and surface species. Figure 5 represents the Mn K-edge XANES spectra for **LT** and **HT**, together with those for the references Mn_2O_3 and MnO_2. The edge energies of lithium manganates are found to be lower than that of the Mn^{+IV} reference but higher than that of the Mn^{+III} reference, indicating the mixed oxidation state of manganese (Mn^{+III}/Mn^{+IV}) in these compounds. And it is also observed that an enhancement of the formal valence from $Mn^{+III}{}_2O_3$ to $Mn^{+IV}O_2$ gives rise to a blue-shift of the edge position by 3 eV. In this context, taking into account the XPS result where the oxidation state of manganese is increased by 0.15 as the sintering temperature is decreased from 700 (**HT**) to 250 °C (**LT**), the edge energy of **LT** is expected to be higher by ≥ 0.4 eV than that of **HT**. However, as shown in Figure 5, there is no prominent change in the edge energy between both compounds. Such an inconsistency between XPS and XAS results highlights that the decrease of particle size has a significant influence mainly on the surface species, not on the bulk species. On the basis of such experimental findings and previous observations, it can be argued that the modification of the surface would be closely related to the dependence of the electrochemical efficiency of $LiMn_2O_4$ on synthetic conditions, which is different for the 3 V and 4 V regions. To get a more detailed information on the electronic and geometric structures around the manganese ion, each spectrum has been carefully investigated by using the second differential method which is quite effective in differentiating a small difference of spectral features (the inset of Figure 5). Both spectra of **LT** and **HT** show doubly split preedge peaks (denoted as P_1 and P_2), which are attributed to the quadrupole-allowed transitions from the core 1s level to unoccupied 3d states. Such a splitting of the preedge peak surely originates from the separation of degenerate 3d levels under the octahedral crystal field. In the case of $LiMn_2O_4$ spinel compounds with a weak crystal field, the $1s^1 3d_{t2g}{}^3 3d_{eg}{}^1$ final state, due to the $1s \rightarrow 3d_{eg}$ transition, is expected to be more stable than the $1s^1 3d_{t2g}{}^4 3d_{eg}{}^0$ state resulting from the $1s \rightarrow 3d_{t2g}$ transition, since the crystal field splitting of 10 Dq is smaller than the pairing energy for a weak crystal field ion. Therefore, the lower energy peak, P_1, should be attributed to a transition of $1s \rightarrow 3d_{eg}$, while the higher one, P_2, should be assigned as a transition of $1s \rightarrow 3d_{t2g}$, even though the energy of $3d_{t2g}$ level is lower than that of $3d_{eg}$ level. In fact, such assignments of the preedge peaks are supported by the previous O K-edge XAS study on giant magnetoresistance $La_{0.7}Sr_{0.3}MnO_3$ material.[32] On the basis of the present assignments, a stronger intensity of P_1 compared to P_2 can be well understood by the fact that the $LiMn_2O_4$ compound has a mixed oxidation state with Mn^{+III}/Mn^{+IV}, leading to a lower electron concentration in $3d_{eg}$ orbital than in $3d_{t2g}$ one. In this context, an enhancement of the lower energy peak P_1 upon a decrease of sintering temperature indicates that the oxidation state of manganese is higher for the **LT** sample than for the **HT** sample, resulting in a decrease of electron concentration in the $3d_{eg}$ orbital.

Mn K-Edge EXAFS Analysis. The effect of synthetic temperature on the crystal structure of the $LiMn_2O_4$ spinel oxide has also been investigated by using Mn K-edge EXAFS analysis. The k^3-weighted Mn K-edge EXAFS spectra for **LT** and **HT** are shown in Figure 6a, and the corresponding Fourier transforms (FTs) in the k range of 2.75−13.6 $Å^{-1}$ in Figure 6b. It is clearly observed from Figure 6b that both lithium manganates exhibit two intense peaks at ∼1.6 and ∼2.6 Å, which are attributed to the (Mn−O) and (Mn−Mn) bonding pairs, respectively. These FT peaks were isolated by inverse Fourier transform to k space. The resulting $k^3\chi(k)$ Fourier filtered EXAFS oscillations are represented in Figure 7, and the curve fitting analyses were carried out to them in order to determine the structural parameters such as coordination number (CN), bond distance (R), and Debye−Waller factor (σ^2). The best-fitting results are compared to the experimental spectra in Figure 7, and the fitted structural parameters are listed in Table 2. The (Mn−O) and (Mn−Mn) bond distances are found to be shorter for the **LT** material than for the **HT** material, confirming the higher Mn oxidation state for the former. In addition to the variation in bond distances, the coordination number of manganese is also revealed to decrease with lowering of sintering temperature, which is very consistent with a smaller particle size of **LT**, leading to an unsaturated coordination around Mn near the surface. Such a change in coordination number also implies the possibility of cation mixing between octahedral and tetrahedral sites induced by heat-treatment at lower temperature. This is supported by the fact that the second FT peak corresponding to (Mn−Mn) shell is smaller for **LT** than for **HT**, implying an enhancement of structural disorder around the manganese ion for the former.

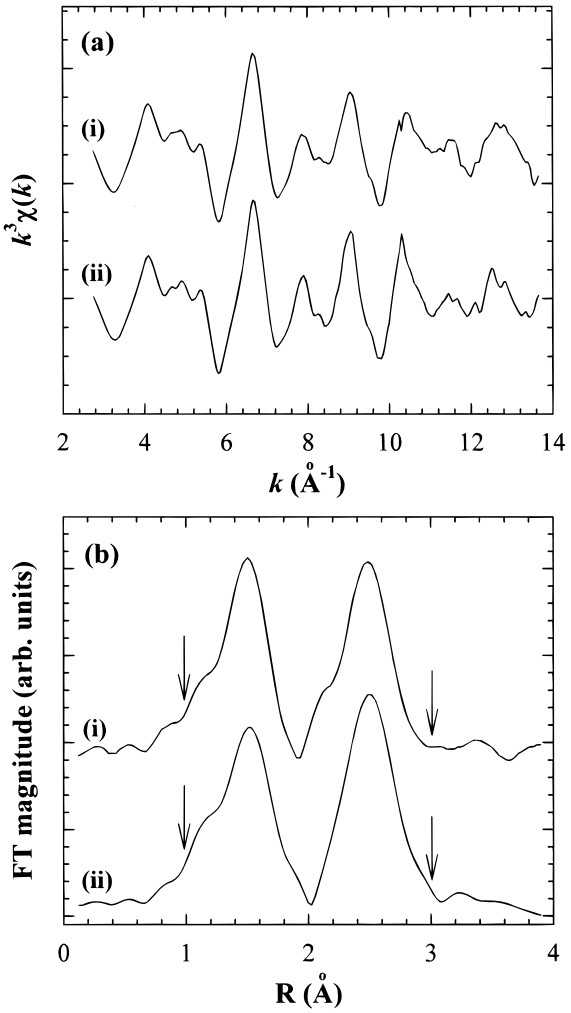

Figure 6. (a) Experimental k_3-weighted Mn K-edge EXAFS spectra and (b) their Fourier transforms for (i) **LT** and (ii) **HT**. The range over which the Fourier filtering has been made is shown by the arrows.

TABLE 2: Results of Non-Linear Least-Squares Curve Fitting for the First and Second Shells of Mn K-Edge EXAFS Spectra for the $LiMn_2O_4$ Spinels, LT and HT, Heated at 250 and 700 °C, Respectively

compound	bond	CN[a]	ΔE_0 (eV)	R (Å)	σ^2 ($\times 10^{-3}$ Å^2)
LT	(Mn−O)	5.6	−2.67	1.90_4	3.35
	(Mn−Mn)	5.2	−4.24	2.88_9	6.24
HT	(Mn−O)	6.0	−3.44	1.91_5	3.99
	(Mn−Mn)	6.0	−3.36	2.89_5	6.41

[a] In order to check out the evolution of coordination number (CN) upon lowering of sintering temperature, all the CN values are determined by using the amplitude reduction factor (S_0^2) of **HT**.

^{7}Li MAS NMR Measurement. For the purpose of elucidating the effect of synthetic temperature on the bonding character of lithium, ^{7}Li MAS NMR measurements have been carried out for the $LiMn_2O_4$ spinels prepared at various temperatures. Since the dipolar contribution of electron spins would be at least partially averaged out under fast MAS conditions, the isotropic position of NMR signals (i.e., Fermi contact shift) is expected to be mainly due to the transfer of some electron density from the Mn 3d orbital to the Li 2s orbital.[22,23] The ^{7}Li NMR spectra for **LT** and **HT** are represented in Figure 8. Both samples exhibit a major resonance at 534 ppm, which is attributed to a lithium ion in the normal tetrahedral 8a site of the spinel structure. In addition, two other resonances are clearly observed for the **HT** sample at 585 and 620 ppm; such additional signals have been

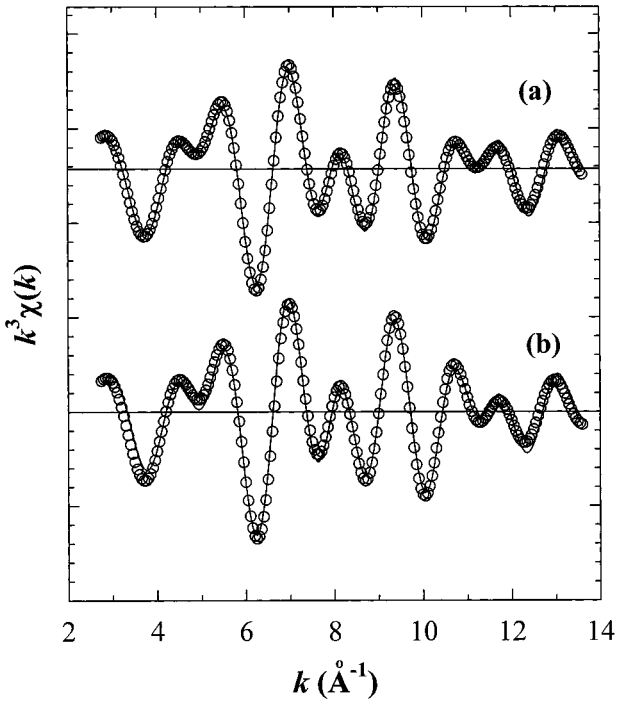

Figure 7. Comparison of the fitted spectra (solid lines) with the experimental data (empty circles) for (a) **LT** and (b) **HT**.

observed in particular by Lee et al.[22] using ^{6}Li NMR on enriched $LiMn_2O_4$ samples, who assigned them to lithium ions near defects which might consist of 16d Mn vacancies. In the case of the **LT** spectrum, these additional signals are rather replaced by a much broader one, which is not completely separated into well-defined spinning sidebands. Such broadening of an additional peak is interpreted as a result of a high Mn oxidation state of **LT**, resulting in a shortening of the Li−Mn bond distance and consequently in an enhancement of interaction between Li and Mn which cannot be averaged by MAS. As shown in Figure 8, it is also discerned that the width of the main peak at 534 ppm is larger for **LT** than for **HT**, suggesting a much broader distribution of Mn^{+III} and Mn^{+IV} around tetrahedral Li^+ in the former due to enhanced cation mixing as probed by EXAFS.

The binding site of intercalated Li^+ ion has been investigated by monitoring the evolution of ^{7}Li MAS NMR spectra upon intercalation of 0.2 mol Li per pristine formula. The MAS NMR spectra of the pristine lithium manganates are compared with those of the corresponding lithium intercalates in Figure 9. The spectral features of **HT** remain nearly the same upon intercalation, except for an appearance of the additional signal at 0 ppm which is attributed to traces of salt from the electrolyte and/or to a passivating film present on the sample surface formed from the decomposition of electrolyte. Taking into account the fact that the Li intercalation may lead to the formation of two phases, i.e., $LiMn_2O_4$ and $Li_2Mn_2O_4$,[1,3] the additional resonances corresponding to the latter phase should be observed near 101 and 118 ppm, as reported previously.[22] However, in the present spectrum of **HT**, such additional signals of $Li_2Mn_2O_4$ seem to be concealed by sidebands of $LiMn_2O_4$ and of the lithium salt (or passivating film), since the amount of newly formed $Li_2Mn_2O_4$ phase is too small to be detected by NMR in the present conditions. On the other hand, the Li insertion into **LT** is found to induce a drastic suppression of the NMR signal, even though only a small amount of Li^+ ion is inserted into the material (0.2 ion per unit formula of $LiMn_2O_4$). In the case of such a nanocrystalline material with many surface defects, the discharge

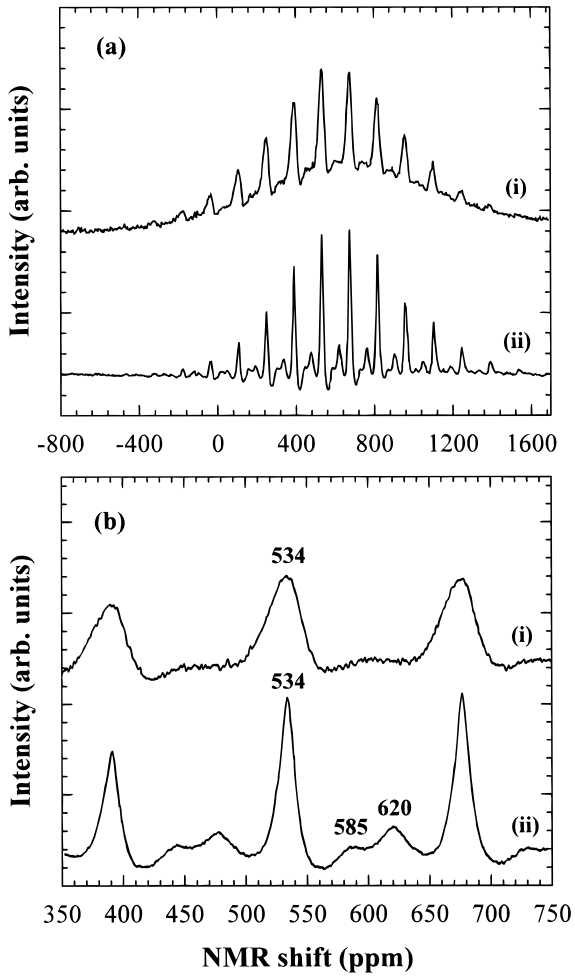

Figure 8. (a) ^{7}Li MAS NMR spectra of (i) **LT** and (ii) **HT**, and (b) the expanded views of the corresponding spectra for the range 350−750 ppm.

process might begin with an electrochemical grafting of Li on these defects, which results in the reduction of surface Mn^{+IV} into surface Mn^{+III}.[10,11] It is well-known that such surface Mn^{+III} ions would be easily dispropotionated into Mn^{+IV} and Mn^{+II} ions through contact with the electrolyte.[33,34] In contrast to the well crystallized spinel where Mn^{+II} ion is mostly dissolved into the electrolyte, the surface defects of **LT** can provide the stable tetrahedral sites for the paramagnetic Mn^{+II} ion that can play an important role in a depression of NMR signal for the lithium ions which would be grafted on the surface.[34] As for the depression of NMR signal, we should also consider the self-disproportionation of stoichiometric $LiMn_2O_4$ into the Li-poor $Li_{1-x}Mn_2O_4$ and the Li-rich $Li_{1+x}Mn_2O_4$, since this reaction has been reported to occur on the surface of the spinel compound.[34] However, in case such a Li-poor phase would be present in the sample (coexisting with Li-rich one), the corresponding well-defined resonance should be observed at 534 ppm. Therefore, this possibility can be ruled out for the present **LT** compound.

The reason why the whole NMR signal should be suppressed by the surface grafting is however not obvious and it requires further investigation. The most probable possibility would be that the grafted Li^+ induces a strong modification in the chemical bonding nature of lithium also in the bulk. Indeed, it is recently understood that the electronic and structural properties of nanocrystalline semiconductors can be drastically changed when species are grafted onto the surface of nanocrystalline materials, for examples, nanocrystalline TiO_2 or In_2O_3 when Ru complexes or ZnO are grafted onto the crystallite surface,

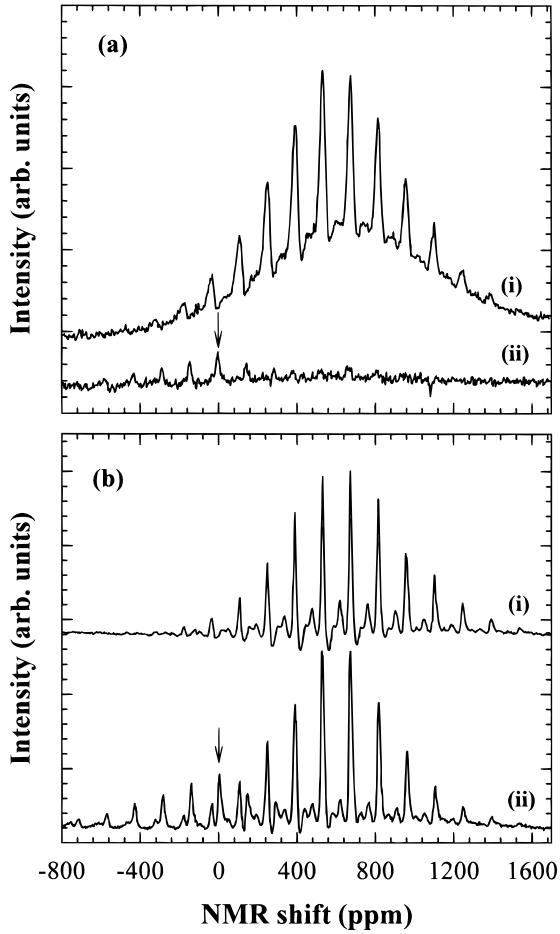

Figure 9. A comparison of ^{7}Li MAS NMR spectra (i) before and (ii) after Li intercalation for (a) **LT** and (b) **HT**. The arrows indicate the additional signals from the trace of salt and/or from a passivating film.

and also nanocrystalline WO_3 electrochemically grafted with H^+ or Li^+.[12]

Conclusions

In the present study, the effects of crystal size on the chemical bonding character and electrochemical property of cathode material have been investigated by performing the systematic XPS, XAS, ^{7}Li NMR analyses, and the electrochemical measurements for the $LiMn_2O_4$ spinel oxides prepared at various temperatures. According to the comparative Mn 2p XPS and Mn K-edge XANES/EXAFS analyses, it is found that the average oxidation state of manganese is enhanced by lowering the sintering temperature, which is more prominent for the surface species than for the bulk ones. And the bonding site of intercalated lithium has been examined by monitoring the evolution of ^{7}Li MAS NMR spectra of $LiMn_2O_4$ before and after Li intercalation. While the intercalation of 0.2 mol of Li per pristine formula does not induce any remarkable spectral change for the microcrystalline sample prepared at 700 °C, it gives rise to a dramatic suppression of the NMR signal of the nanocrystalline sample synthesized at 250 °C, which might account for the Li grafting process. From the present experimental findings, it is concluded that the lowering of the synthetic temperature modifies the surface properties in favor of a grafting process, which is closely related to the enhancement of electrochemical properties for the 3 V region.

Acknowledgment. This work was supported in part by the Institute of Information Technology and Assessment (IITA). G.

Campet is grateful to the Centre National d'Etudes des Telecommunications (CNET) for financial support and technical assistance. J. H. Choy is grateful to the Ministry of Education (BSRI-98-3413) for financial support. The synchrotron radiation experiments at PLS were supported in part by MOST and POSCO.

References and Notes

(1) Thackeray, M. M.; David, W. I. F.; Bruce, P. G.; Goodenough, J. B. *Mater. Res. Bull.* **1983**, *18*, 461.

(2) Thackeray, M. M.; De Kock, A.; Rossouw, M. H.; Liles, D. C.; Hoge, D.; Bittihn, R. *J. Electrochem. Soc.* **1992**, *139*, 363.

(3) Thackeray, M. M. *Prog. Solid State Chem.* **1997**, *25*, 1.

(4) Tarascon, J. M.; Wang, E.; Shokoohi, F. K.; McKinnon, W. R.; Colson, S. *J. Electrochem. Soc*. **1991**, *138*, 2859.

(5) Robertson, A. D.; Lu, S. H.; Averill, W. F.; Howard, W. F., Jr. *J. Electrochem. Soc.* **1997**, *144*, 3500.

(6) Pistoia, G.; Wang, G.; Wang, C. *Solid State Ionics* **1992**, *58*, 285.

(7) Arora, P.; Popov, B. N.; White, R. E. *J. Electrochem. Soc.* **1998**, *145*, 807.

(8) Liu, W.; Kowal, K.; Farrington, G. C. *J. Electrochem. Soc.* **1998**, *145*, 459.

(9) Treuil, N.; Portier, J.; Campet, G.; Ledran, J.; Frison, J. C. **1998**, French patent; European patent number 97402433.3-2111.

(10) Treuil, N. Ph D. Thesis. University Bordeaux-I: France, 1998.

(11) During the discharge process for nanocrystalline $LiMn_2O_4$, the "subband-gap" energy state corresponding to the surface Mn^{+IV} ion is expected to be occupied first by an injected electron, which induces the Li grafting on the surface oxygen at the vicinity of reduced surface Mn. Such a grafting process is followed by the intercalation of Li^+ ions into the crystallite. Since the structural defect or distortion at/near the surface can act as a reversible grafting site, the nanocrystalline material with many surface defects would exhibit a better electrochemical activity than its microcrystalline homologue, in case that the first electrochemical process is a discharge of the Li battery.

(12) Choy, J. H.; Kim, Y. I.; Kim, B. W.; Campet, G.; Portier, J.; Huong, P. V. *J. Solid State Chem.* **1999**, *142*, 368.

(13) Choy, J. H.; Hwang, S. J.; Park, N. G. *J. Am. Chem. Soc.* **1997**, *119*, 1624.

(14) Choy, J. H.; Kim, D. K.; Seung, D. Y.; Levasseur, A. *J. Phys. Chem. Solids*, **1998**, *59*, 1579.

(15) Choy, J. H.; Kim, D. H.; Kwon, C. W.; Hwang, S. J.; Kim, Y. I. *J. Power Sources* **1999**, *77*, 1.

(16) Ammundsen, B.; Jones, D. J.; Roziere, J. *Chem. Mater.* **1996**, *8*, 2799.

(17) Liu, R. S.; Jang, L. Y.; Chen, J. M.; Tsai, Y. C.; Hwang, Y. D.; Liu, R. G. *J. Solid State Chem.* **1997**, *128*, 326.

(18) Kumagai, N.; Fujiwara, T.; Tanno, K.; Horiba, T. *J. Electrochem. Soc.* **1996**, *143*, 1007.

(19) Di Castro, V.; Polzonetti, G.; Contini, G.; Cozza, C.; Paponetti, B. *Surf. Interface Anal.* **1990**, *16*, 571.

(20) Kanzaki, Y.; Taniguchi, A.; Abe, M. *J. Electrochem. Soc.* **1991**, *138*, 333.

(21) Morgan, K. R.; Collier, S.; Burns, G.; Ooi, K. *J. Chem. Soc., Chem. Commun.* **1994**, 1719.

(22) Lee, Y. J.; Wang, F.; Grey, C. P. *J. Am. Chem. Soc.* **1998**, *120*, 12601−12613, and reference therein.

(23) Gee, B.; Horne, C. R.; Cairns, E. J.; Reimer, J. A. *J. Phys. Chem. B* **1998**, *102*, 10142−10149.

(24) Marichal, C.; Hirschinger, J.; Granger, P.; Menetrier, M.; Rougier, A.; Delmas, C. *Inorg. Chem.* **1995**, *34*, 1773.

(25) Saadoune, I.; Menetrier, M.; Delmas, C. *J. Mater. Chem.* **1997**, *7*, 2505.

(26) Mustarelli, P.; Massaroti, V.; Bini, M.; Capsoni, D. *Phys. Rev. B* **1997**, *55*, 12018.

(27) Moulder, J. F.; Stickle, W.; Sobol, P.; Bomben, K. D. *Handbook of X-ray Photoelectron Spectroscopy*; Perkin-Elmer: Eden Prairie, MN, 1992.

(28) Lytle, F. W.; van der Laan, G.; Greegor, R. B.; Larson, E. M.; Violet, C. E.; Wong, J. *Phys. Rev. B* **1990**, *41*, 8955.

(29) Stern, E.-A.; Kim, K. *Phys. Rev. B* **1981**, *23*, 3781.

(30) Teo, B. K. *EXAFS: Basic Principles and Data Analysis*; Springer-Verlag: Berlin, 1986.

(31) It should be noted that the present oxidation states correspond to the manganese species on the surface. And moreover, these values would be rather underestimated, since the spectrum of the reference Mn_2O_3 contains a small amount of an Mn^{+IV} component.

(32) Park, J. H.; Kimura, T.; Tokura, Y. *Phys. Rev. B* **1998**, *58*, R13330.

(33) Gummow, R. J.; de Kock, A.; Thackeray, M. M. *Solid State Ionics* **1994**, *69*, 59.

(34) Thackeray, M. M.; Mansuetto, M. F.; Bates, J. B. *J. Power Sources* **1997**, *68*, 153.